

# Variational Approach to Vector Field Decomposition

Konrad Polthier and Eike Preuß

Technische Universität Berlin  
{polthier, preuss}@math.tu-berlin.de

**Abstract.** For the feature analysis of vector fields we decompose a given vector field into three components: a divergence-free, a rotation-free, and a harmonic vector field. This Hodge-type decomposition splits a vector field using a variational approach, and allows to locate sources, sinks, and vortices as extremal points of the potentials of the components. Our method applies to discrete tangential vector fields on surfaces, and is of global nature. Results are presented of applying the method to test cases and a CFD flow.

## 1 Introduction

Features of vector fields strongly affect the characteristics of flows and their physical behavior. Among the most important features are vortices and pairs of sources and sinks. In many applications, vortices must be avoided to avoid energy losses, or sources and sinks must be located, for example to understand atmospheric behaviors. Although feature analysis is an important area only few technical tools are available for their detection and visualization.

A number of heuristic criteria are currently used for vortex detection [11][6]. Physical quantities of the underlying grid such as vortex magnitude and helicity are located at isolated vertices of the grid. Such local characterizations depend on the chosen neighbourhood and have deficiencies in regions with lower flow velocity. A slightly more global approach analyses the behaviour of streamlines and other integral curves. For example, geometric quantities derived from curvature properties of streamlines are used by Sadarjoen and Post [14] to find vortex cores, and the polyhedral winding angle of a discrete streamline in [13] is used to detect closed streamlines around a possible vortex core. Topological methods as introduced by Helman and Hesselink [5] try to decompose vector fields in different global regions of interest by computing integral curves from critical points found by local linear approximations of the Jacobian. Higher-order approximations yield different decomposition [15][7]. For an overview of known methods in vector field visualization see Teitzel [16].

In this paper we present a variational approach for the decomposition of a given vector field in different components, a divergence-free, a rotation-free, and a harmonic remainder. Instead of trying to define a discrete version of the Jacobian  $\nabla\xi$

---

<sup>0</sup> to appear in: Eurographics Workshop on Visualization, Springer Verlag 2000

of the discrete vector field and its splitting in a stretching tensor  $S$  and a vorticity matrix  $\Omega$ , we derive a Hodge type decomposition by minimizing certain energies. This more global point of view reduces the dependency on local measurement inaccuracies and discretization artifacts. Our approach comes along the lines with a definition of discrete differential operators of higher differentiability order on piecewise linear functions and vector fields [9].

The application of our decomposition is two-fold. First, the derived vector field components have distinguished properties which are mixed in the original vector field. Second, two components are the gradient respectively the co-gradient of potential functions. The existence of potential functions allows to identify features of the original vector field as local extrema of the associated potentials which are easily detectable.

## 2 Related Work

Methods for direct vortex detection are often based on the assumption to have regions with high amounts of rotation or of pressure extrema. See for example Banks and Singer [1] for an overview of possible quantities to investigate. The deficiencies of first-order approximations have been widely recognized, and, for example, tried to overcome with higher-order methods [12][15].

The Jacobian  $\nabla\xi$  of a differentiable vector field  $\xi$  in  $\mathbb{R}^2$  and  $\mathbb{R}^3$  can be decomposed in a stretching tensor  $S$  and a vorticity matrix  $\Omega$

$$\nabla\xi = \frac{1}{2}(\nabla\xi + \nabla\xi^t) + \frac{1}{2}(\nabla\xi - \nabla\xi^t) =: S + \Omega.$$

The eigenvalues of the diagonal matrix  $S$  correspond to the compressibility of the flow, and the off-diagonal entries of the anti-symmetric matrix  $\Omega$  are the components of the rotation vector.

In the present paper we choose a different approach by defining higher order differential operators. On discrete curved surfaces it is rather non-trivial to define higher order derivatives point-wise and in local coordinates. Therefore we follow a different approach and define discrete differential operators as total quantities being integrated over local regions. For example, the discrete divergence of a vector field is defined at an edge midpoint as an integrated quantity over the adjacent triangles. Similar concepts are, for example, used for the (total) Gauß curvature at vertices of polyhedral surfaces [10].

On the other hand, our approach has contact with weak derivatives used in finite element theory where the formal application of partial integration is used to shift the differentiation operation to differentiable test functions. In fact, the integrands of our discrete differential operators  $\text{div}_h$  and  $\text{rot}_h$  have been obtained from  $\nabla\xi$  by formal partial integration with test functions.

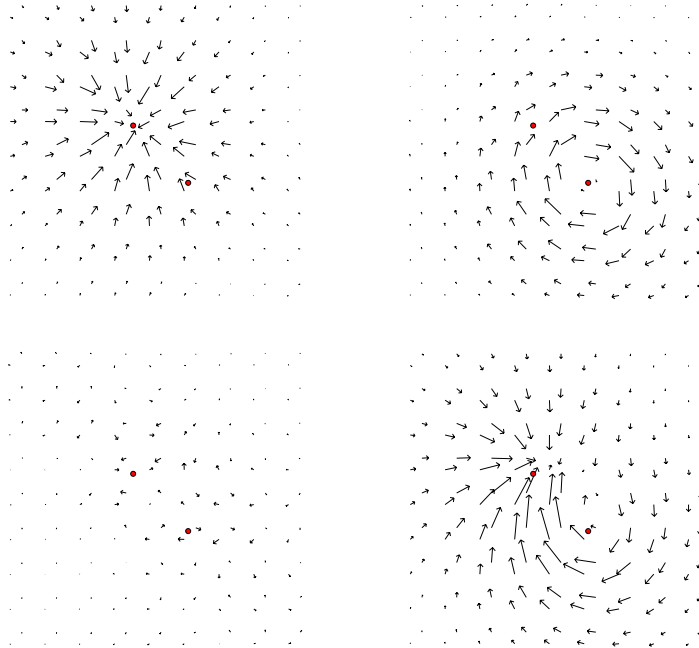


**Fig. 1.** Decomposition of test vector field (bottom right) in rotation-free (upper left), divergence-free (upper right) and harmonic component (bottom left). The two dots in each image indicate the centers of the original potential. Notice, that the dots in the combined vector field do not seem to lie in the centers indicated by the vector field, although they do. But the components clearly recover the original centers. Compare figure 3 for the associated potentials.

We avoid the derivation of the more technical details of the vector field decomposition and prefer to cite the important theorems in section 3. A discussion of the experimental results is given in section 4 where we discuss the decomposition of different test cases.

### 3 Decomposition of Discrete Vector Fields

In this section we are heading for a decomposition of tangential vector fields in  $\Lambda^1$  into simpler components with special properties. A vector field in  $\Lambda^1$  is integrable if it is the gradient of a function in  $S_h$ . To define other types of vector fields let us recall some differential operators and define discrete equivalents. For details of this section we refer to [9].

Let  $\mathfrak{T}$  be the triangulation of a curved surface immersed in  $\mathbb{R}^3$  (or more general,  $\mathbb{R}^n$ ) which is assumed to be simply connected, for simplicity. On  $\mathfrak{T}$  we have the

function space

$$S_h := \left\{ u \mid \begin{array}{l} u|_T \text{ is a piecewise linear function on each triangle } T \in \mathfrak{T}, \\ \text{and } u \text{ is continuous on } \mathfrak{T} \end{array} \right\}.$$

of piecewise linear functions. They are uniquely determined by their values at vertices. We consider the space of piecewise constant vector fields

$$\Lambda^1 := \{ \xi \mid \xi|_T \text{ is a constant, tangential vector on each triangle } T \in \mathfrak{T} \}.$$

The divergence of a differentiable vector field  $v = (v_1, v_2)$  in the euclidean plane with respect to local coordinates  $(x, y)$  is defined as  $\operatorname{div} v = v_{1|x} + v_{2|y}$ , and the rotation is a vector of length  $|\operatorname{rot} v| = v_{2|x} - v_{1|y}$  normal to the plane. Recalling that for a vertex  $p \in \mathfrak{T}$ , the set  $\operatorname{star} p$  consists of all triangles having  $p$  as vertex, and for an edge midpoint  $m$ ,  $\operatorname{star} m$  consists of the two triangles having  $m$  in common, we define discrete versions of both differential operators, the discrete divergence and the discrete rotation:

**Definition 1.** *Let  $\xi$  be a piecewise constant vector field on  $\mathfrak{T}$ . Then the discrete divergence respectively discrete rotation of  $\xi$  are defined at each edge midpoint  $m$  by*

$$\begin{aligned} \operatorname{div}_h \xi(m) &:= \int_{\partial \operatorname{star} m} \langle \xi, \nu \rangle \\ \operatorname{rot}_h \xi(m) &:= \int_{\partial \operatorname{star} m} \langle J\xi, \nu \rangle \end{aligned}$$

where  $J$  denotes the rotation of a vector by  $90^\circ$  degrees in the plane of a triangle, and  $\nu$  the exterior normal along the oriented boundary of  $\operatorname{star} m$ .

Our main application of the discrete differential operators is the characterization of integrable vector fields. We recall that a smooth vector field  $\xi$  is gradient of a differentiable function if and only if its rotation vanishes, and, correspondingly,  $J\xi$  is gradient if the divergence of  $\xi$  vanishes. In the discrete setting we have a similar result:

**Theorem 1.** *Let  $\xi \in \Lambda^1$  be a piecewise constant vector field on a simply connected triangulation  $\mathfrak{T}$ . Then we have*

1.  $\xi = \nabla u$  with a function  $u \in S_h$  if and only if  $\operatorname{rot}_h \xi(p) = 0$
2.  $\xi = J\nabla w$  with a function  $w \in S_h$  if and only if  $\operatorname{div}_h \xi(p) = 0$ .

This result leads to the possibility of decomposing a vector field on triangulated surfaces in a rotation-free, a divergence-free, and a harmonic vector field.

**Theorem 2.** *Let  $\mathfrak{T}$  be a triangulation of a compact surface. Any vector field  $\xi \in \Lambda^1(\mathfrak{T})$  has a unique decomposition*

$$\xi = \nabla u + J\nabla w + v$$

with  $u, w \in S_h$ ,  $v \in \Lambda^1$  and normalization

$$\int_{\Omega} u = 0, \int_{\Omega} w = 0 \text{ and } \operatorname{div}_h v = 0, \operatorname{rot}_h v = 0.$$

The function  $u$  respectively  $w$  is obtained by minimizing the energy determined by the value  $\langle \nabla u - 2\xi, \nabla u \rangle$  respectively  $\langle \nabla w + 2J\xi, \nabla w \rangle$  integrated over  $\mathfrak{T}$ . The harmonic vector field component  $v$  is defined as the remainder  $v := \xi - \nabla u - J\nabla w$ . The normalization of  $u$  and  $w$  only fixes a specific offset, and it has no influence on the gradients.

In our numerical experiments the energy minimization is performed with a conjugate gradient method leading to minimizers  $u$  and  $w$  in  $S_h$  of the respective energies. These functions directly determine the three vector field components  $\nabla u$ ,  $J\nabla w$ , and  $v$ . Please note, for efficiency, one does not need to store the three components explicitly since they are determined by the scalar-valued potential functions  $u$  and  $w$ . Further, if one is interested only, say, in identifying the vortices of a vector field  $\xi$ , then it suffices to calculate  $w$  and identify its local extrema, i.e. without actually performing the decomposition.

## 4 Results

The first test case consists of an artificial vector field generated as the sum of a gradient vector field corresponding to a point potential and three rotation vector fields corresponding to three potentials whose gradient has been rotated by 90° degrees, see figure 2. Application of the minimization algorithms leads to two functions  $u$  and  $w$ . The upper images in figure 2 display  $\nabla u$  and  $J\nabla w$ . The algorithm has clearly separated the gradient field from the three vortices.

The visualization is made with the line integral convolution method [2]. We used a filter kernel with variable length to emphasize regions with vectors of small length.

Another interesting fact is visible in figure 1 where the original vector field is the sum of a single potential and vortex. The two dots in each image indicate the centers of the original potentials. Notice, that the dots in the combined vector field seem to deviate from the centers indicated by the vector field, although they do are in the correct place. Obviously, the summation of both vector fields leads to a misleading transition of the visible vortex center and potential. It is remarkable, that the reconstructed components clearly recover the original centers.

We have applied the algorithm to a flow from a CFD simulation, see figure 4. The rotation-free component of the incompressible flow around a cylinder vanishes as

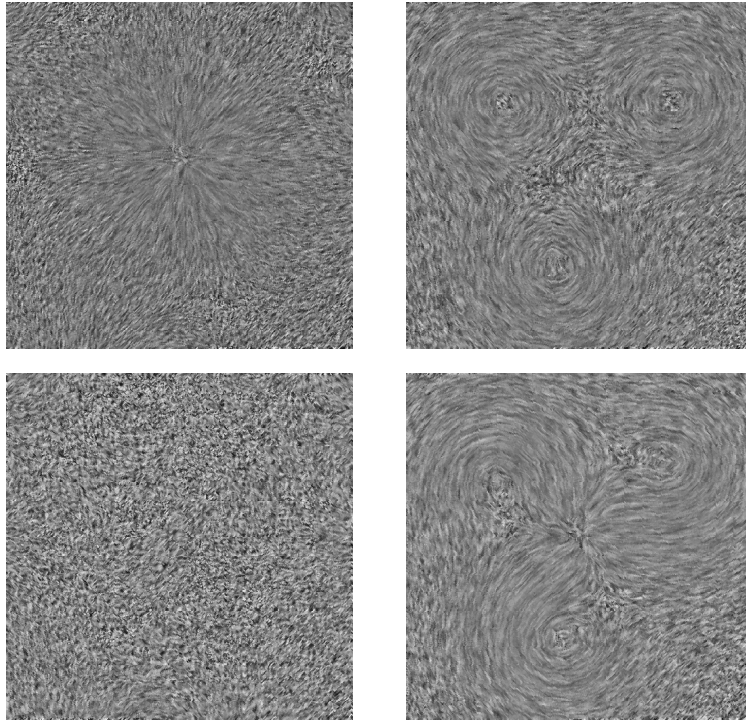


**Fig. 2.** Test vector field consisting of three vortices and a potential. The algorithm clearly separates the components. The harmonic component (lower left) has only a minor size.

expected, except at inlet and outlet. The divergence-free component has additional artifacts at the boundary which are currently not well-understood.

A slight drawback of the present method is that it does not allow interaction of the user to steer the decomposition. Compare de Leeuw and Post [3] for interactive vortex detection.

Leeuw and van Liere [4] proposed a hierarchical ordering of flow features to reduce the complexity and suppress high-frequency patterns. It would be an interesting approach to combine their ideas with the decomposed fields presented here. An approach might be to first smooth the obtained principal functions to reduce high-frequencies.

The vector field components derived from gradients of the potentials are directed, and, therefore, emphasizing the vector directions in the LIC images will enroll additional information. Here tools for displaying the orientation of vectors using oriented textures developed in [8] would clearly add information to the LIC images.

## 5 Conclusions and Future Work

We have presented a variational approach for the decomposition of piecewise linear and piecewise constant vector field on triangulated surfaces in a divergence-free and

a rotation-free component with a harmonic remainder. In many sample cases we obtained a nearly perfect separation of different features. We notice that in test cases with incompressible flows the divergence-free component vanishes as expected, but the harmonic remainder has a significant size. Here future study must concentrate on the currently unclear physical properties and features associated with the harmonic component.

The existence of different components of the vector field enables to separate features of the vector field, and study them for each component separately. Beside an extension to three-dimensional flows in volumes, there is also a connection to other feature extraction concepts required. Especially useful should be that fact, that the decomposition allows to study the potentials associated with the components rather than the vector fields as indicated in figure 3.

## References

1. D. Banks and B. Singer. A predictor-corrector technique for visualizing unsteady flow. *IEEE Transactions on Visualization and Computer Graphics*, 1(2):151–163, June 1995.
2. B. Cabral and L. C. Leedom. Imaging vector fields using line integral convolution. *SIGGRAPH 93 Conference Proceedings*, 27:263–272, 1993.
3. W. C. de Leeuw and F. H. Post. A statistic view on vector fields. In M. Göbel, H. Müller, and B. Urban, editors, *Visualization in Scientific Computing, Eurographics*, pages 53 – 62, Wien, 1995. Springer Verlag.
4. W. C. de Leeuw and R. van Liere. Visualization of global flow structures using multiple levels of topology. In E. Gröller, H. Löffelmann, and W. Ribarsky, editors, *Data Visualization '99*, pages 45 – 52. Springer Verlag, 1999.
5. J. Helman and L. Hesselink. Representation and display of vector field topology in fluid flow data sets. *Computer*, 22(8):27–36, August 1989.
6. D. Kenwright and R. Haimes. Vortex identification - applications in aerodynamics: A case study. In R. Yagel and H. Hagen, editors, *Proc. Visualization '97*, pages 413 – 416, 1997.
7. D. N. Kenwright, C. Henze, and C. Levit. Feature extraction of separation and attachment lines. *IEEE Trans. on Visualization and CG*, 5(2):135–144, 1999.
8. L. Khouas, C. Odet, and D. Friboulet. 2d vector field visualization using furlike texture. In E. Gröller, H. Löffelmann, and W. Ribarsky, editors, *Data Visualization '99*, pages 35 – 44. Springer Verlag, 1999.
9. K. Polthier. Hodge decomposition of vectorfields. *in preparation*, 1999.
10. K. Polthier and M. Schmies. Straightest geodesics on polyhedral surfaces. In H.-C. Hege and K. Polthier, editors, *Mathematical Visualization*, pages 135–150. Springer Verlag, Heidelberg, 1998.
11. M. Roth and R. Peikert. Flow visualization for turbomachinery design. In R. Yagel and G. Nielson, editors, *Proc. Visualization '96*, pages 381 – 384. IEEE Computer Society Press, 1996.
12. M. Roth and R. Peikert. A higher-order method for finding vortex core lines. In D. Ebert, H. Hagen, and H. Rushmeier, editors, *Proc. Visualization '98*, pages 143 – 150. IEEE Computer Society Press, 1998.
13. I. Sadarjoe, F. Post, B. Ma, D. Banks, and H. Pagendarm. Selective visualization of vortices in hydrodynamic flows. In D. Ebert, H. Hagen, and H. Rushmeier, editors, *Proc. Visualization '98*, pages 419 – 423. IEEE Computer Society Press, 1998.
14. I. Sadarjoe and F. H. Post. Geometric methods for vortex extraction. In E. Gröller, H. Löffelmann, and W. Ribarsky, editors, *Data Visualization '99*, pages 53 – 62. Springer Verlag, 1999.
15. G. Scheuermann, H. Hagen, and H. Krüger. Clifford algebra in vector field visualization. In H.-C. Hege and K. Polthier, editors, *Mathematical Visualization*, pages 343–351. Springer-Verlag, Heidelberg, 1998.

16. C. Teitzel. Adaptive methods and hierarchical data structures for interactive three-dimensional flow visualization. Dissertation, Friedrich-Alexander-Universität Erlangen-Nürnberg, IMMD 32/09, Computer Graphics Group, September 1999.

## 6 Figure Appendix

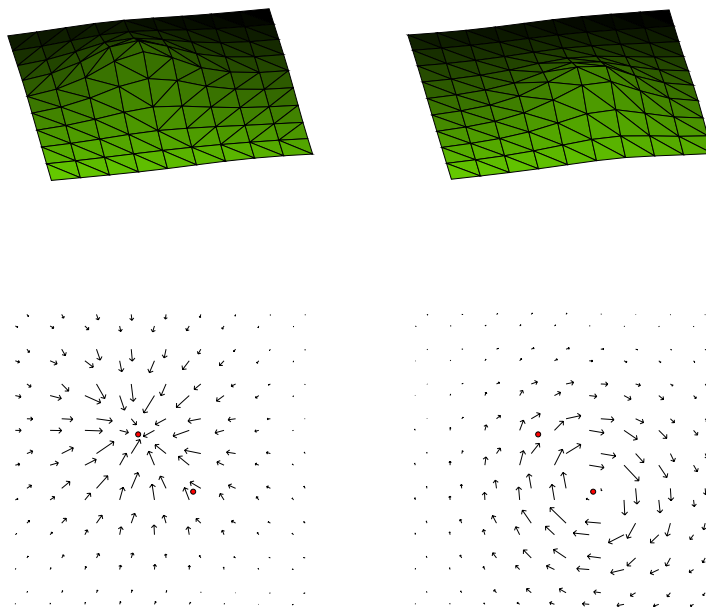


**Fig. 3.** Rotation-free (left column) and divergence-free (right column) components of the vector field decomposition shown in figure 1 with associated potentials. Features of the original vector field are easily identified as local extrema of the potentials.

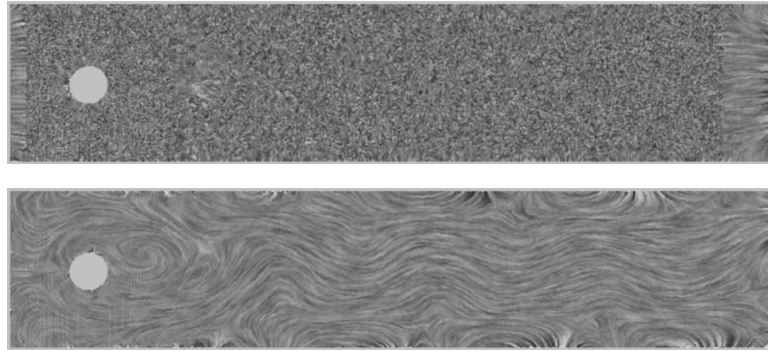


**Fig. 4.** Incompressible flow around a cylinder. Rotation-free component (top) vanishes except at inlet and outlet. Divergence-free component (bottom) has additional artifact at boundary. Courtesy Michael Hinze, TU-Berlin.

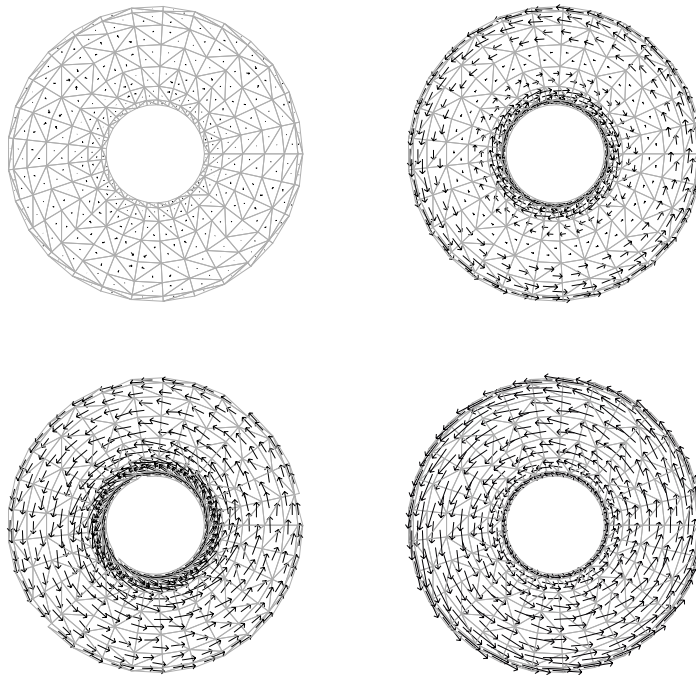


**Fig. 5.** Decomposition of the vector field generated by rotating the torus around the vertical axis (bottom right). The rotation-free component (upper left) vanishes because the field belongs to an isometry of the ambient space. Since the torus is not-simply connected we have a typical harmonic component (bottom left) belonging to the incompressible, rotation-free component of the underlying flow. The divergence free component (upper right) shows the expected behavior where the vortex maxima are a one-parameter family along the upper and lower latitudes.